Journal of Electroanalytical Chemistry 908 (2022) 116118

Contents lists available at ScienceDirect

Journal of Electroanalytical Chemistry

journal homepage: www.elsevier.com/locate/jelechem

Energy storage performance of LiV_3O_8/water-in-salt electrolyte/$LiNi_{1/3}Co_{1/3}Mn_{1/3}O_2$ cell for aqueous lithium-ion batteries

Muharrem Kunduraci [a,*], Selda Kilic Cetin [b], Ugur Caglayan [c], Rasiha Nefise Mutlu [d], Dogan Kaya [e], Ahmet Ekicibil [b]

[a] Department of Aerospace Engineering, Tarsus University, Mersin, Turkey
[b] Department of Physics, Faculty of Sciences and Letters, Cukurova University, Adana, Turkey
[c] Central Research Laboratory, Cukurova University, Adana, Turkey
[d] Department of Chemistry, Faculty of Arts and Science, Mersin University, Mersin, Turkey
[e] Department of Electronics and Automation, Vocational School of Adana, Cukurova University, Adana, Turkey

ARTICLE INFO

Keywords:
Aqueous electrolyte
Lithium-ion battery
Cathode
Anode
Water-in-salt

ABSTRACT

Electrochemical performance of an aqueous lithium-ion battery containing LiV_3O_8 anode, 'water-in-salt' 20 M LiTFSI electrolyte and $LiNi_{1/3}Co_{1/3}Mn_{1/3}O_2$ cathode was studied. In the full cell, the cathode and anode reached a maximum lithiation capacity of 145.8 mAh g^{-1} and 80 mAh g^{-1}, respectively. The full cell successfully underwent 100–110 cycles before hitting 20% capacity loss limit. The average discharge potential of the cell started at 0.849 V and stayed relatively stable in the next 140 cycles. The first cycle coulombic efficiency was as high as 80% and it stabilized at 99–100% in the subsequent cycles. These are the best numbers ever reported for this anode/cathode couple. This outperformance was achieved thanks to the increased stability of the anode and cathode materials in high molarity 'water-in-salt' electrolyte over lower molarity nitrate or sulfate electrolytes previously reported in literature.

1. Introduction

Aqueous lithium-ion batteries (LiB) have the potential to replace traditional organic-based LiB as they offer improved thermal safety, lower material and manufacturing costs and no toxicity. Despite such advantages, several anode [1–5] and cathode [6–9] materials were proposed and tested with limited success since the first demonstration of aqueous LiB in 1994 [10]. Among the cathodes, spinel-type $LiMn_2O_4$ and olivine-type $LiFePO_4$ seem to be much more favored than nickel-based layered-type $LiNi_aCo_bMn_cAl_dO_2$ materials. This is probably due to the high moisture sensitivity of nickel-based cathodes, thereby resulting in poor reversibility in aqueous electrolytes. However, Kunduraci et al., [11] recently demonstrated that $LiNi_{0.6}Co_{0.2}Mn_{0.2}O_2$ can reach a discharge capacity of 152 mAh g^{-1} in water-in-salt 20 M LiTFSI electrolyte with good stability, unlike aqueous nitrate or sulfate electrolytes. This outperformance in high molarity LiTFSI electrolyte was based on the improvement in the surface structural stability of layered cathode resulting from reduced number of free water molecules in the electrolyte.

In this work, we proceeded further with the previous study and demonstrate here a LiV_3O_8/$LiNi_{1/3}Co_{1/3}Mn_{1/3}O_2$ full cell with good cycling stability. LiV_3O_8 has been widely used as positive electrode material in non-aqueous LiB [12–13] and as negative electrode material in aqueous LiB [14–15] due to its easy synthesis, high lithiation capacity and low cost. In fact, LiV_3O_8 anode was previously coupled with several layered cathodes such as $LiCoO_2$ [16,17], $LiNi_{1/3}Co_{1/3}Mn_{1/3}O_2$ [18,19] and $LiNi_{0.81}Co_{0.19}O_2$ [20] in aqueous solutions of $LiNO_3$ and Li_2SO_4 electrolytes. However, the anode and cathode capacities were rather low and the cells did not survive more than 20 cycles. Wang et al., [19] reported in 2011 that the reversibility of LiV_3O_8/$LiNi_{1/3}Co_{1/3}Mn_{1/3}O_2$ couple became better with increasing $LiNO_3$ molarity in aqueous electrolyte and the best performance was achieved in saturated $LiNO_3$ solution. Their results are well agreed with our previous finding that the cyclability of active materials in aqueous electrolytes improve with the reduced availability of free water molecules enabled by larger salt concentrations. Xu et al., [21] recently reported an aqueous solution using 20 M LiTFSI salt and coined the term 'water-in-salt' electrolyte. By taking advantage of this

* Corresponding author.
E-mail address: kunduraci.m@hotmail.com (M. Kunduraci).

https://doi.org/10.1016/j.jelechem.2022.116118
Received 18 November 2021; Received in revised form 2 February 2022; Accepted 2 February 2022
Available online 5 February 2022

concept, it has been shown in this study that the cycle life of this anode/cathode couple can be extended to 100–110 cycles before 20% loss limit is reached, thereby significantly exceeding previous studies.

2. Experimental

2.1. Synthesis of LiV_3O_8

LiV_3O_8 was synthesized by sol–gel method using high purity chemicals of LiOH and NH_4VO_3 as starting compounds. The stoichiometric amounts of precursor LiOH was dissolved in dilute water and NH_4VO_3 was dissolved in a mixture of water and oxalic acid (twice the total mole of Li and V). These solutions were mixed in a magnetic stirrer with heating at 80°C. At the end of the 12 h heating and mixing process, the heat treatment was applied for 1 h in the oven at 300°C and the material turned into a powder form. Then, the powder was heated at 500°C in ambient air for 6 h.

2.2. Synthesis of $LiNi_{1/3}Co_{1/3}Mn_{1/3}O_2$

$LiNi_{1/3}Co_{1/3}Mn_{1/3}O_2$ was synthesized by Pechini method. The required amounts of Co(II) nitrate hexahydrate, Mn(II) nitrate tetrahydrate and Ni(II) nitrate hexahydrate salts were dissolved in 3 mL of distilled water. The aqueous solution was added dropwise to citric acid–ethylene glycol (1:4 mol ratio) solution kept at 90 °C until completion. The solution, which turned more viscous with time, was heated to 150 °C for esterification. After all water was removed and esterification was finished, the solution turned into solid chunk. The fully dried solid was ground and initially heated to 500 °C for 1 h in air to burn the organics and finally to 825 °C for 10 h in air to obtain crystalline structure.

2.3. Structural and morphological analyses

Crystal structure analyses of LiV_3O_8 and $LiNi_{1/3}Co_{1/3}Mn_{1/3}O_2$ were performed by PANalytical Empyrean X-ray diffractometer using CuKα radiation. The diffraction patterns were collected between $2\theta = 10^\circ$ and 70° at a scan rate of 2 ° min^{-1}. The morphological features of materials were observed with FIA-Quanta FEG 650 model scanning electron microscope (SEM). The oxidation states of Mn, Ni and Co in $LiNi_{1/3}Co_{1/3}Mn_{1/3}O_2$ and V in LiV_3O_8 were determined by X-ray photoelectron spectrometer (XPS, PHI 5000 VersaProbe). The peak positions were calibrated by referencing the C1s peak position at 284.8 eV and shifting other peaks in the spectrum accordingly.

2.4. Electrode preparation and electrochemical testing

In order to prepare the anode and cathode slurries, 200 mg of active material (LiV_3O_8 or $LiNi_{1/3}Co_{1/3}Mn_{1/3}O_2$), 25 mg of Timcal Super C45 conductive carbon, 25 mg of Polyvinylidene fluoride and 1.5 g of *N*-Methyl-2-pyrrolidone (NMP) were placed inside a vial. After 1 h of magnetic stirring at 500 rpm, a few drops of each slurry was cast onto pre-cleaned 1 cm^2 Titanium disk to prepare anode and cathode electrodes. The NMP solvent was removed after keeping the Ti foil at 120 °C overnight.

For non-aqueous battery testing of LiV_3O_8 sample, 2032 coin cells were prepared in an Ar-filled glovebox with H_2O and O_2 levels under 1 ppm. Lithium foil was used as counter electrode with 1 M $LiPF_6$ dissolved in EC-DEC as electolyte and Whatman glass fiber paper as separator. The cells were galvanostatically charged and discharged between 1.8 V and 4.0 V vs. Li.

The aqueous half cell measurements were performed in open air in 10 mL 20 M Lithium bistrifluoromethanesulfonimide (LiTFSI) aqueous electrolyte. Pt and Ag/AgCl electrodes were used as counter and reference electrodes, respectively. The selected voltage range was −0.25 V − 0.70 V vs. Ag/AgCl for LiV_3O_8 and 0 V − 1.2 V vs. Ag/AgCl for $LiNi_{1/3}Co_{1/3}Mn_{1/3}O_2$. Charge and discharge rates were 25 mA g^{-1} based on active material weight. The three electrode cyclic voltammetry measurements of these cells were performed using the same counter and reference electrodes, aqueous electrolyte and voltage ranges at a scanning rate of 0.1 mV s^{-1}.

For aqueous battery testing of full cells, 2032 coin cells were prepared in open air. They contained LiV_3O_8 as anode, $LiNi_{1/3}Co_{1/3}Mn_{1/3}O_2$ as cathode, 20 M LiTFSI as aqueous electrolyte and glass fiber paper as separator. The weight ratio of LiV_3O_8 to $LiNi_{1/3}Co_{1/3}Mn_{1/3}O_2$ in the full cell was 2.26 (6.16 mg anode and 2.72 mg cathode). The cells were galvanostatically charged and discharged between 0.2 V and 1.4 V for a total of 140 cycles. The current rate was 25 mA g^{-1} based on the weight of cathode active material. At the end of this cycling protocol, the rate performance of the full cell was evaluated at *C*/4, *C*/2, 1*C*, 2*C* and 4*C* discharge rates in sequence.

3. Results

3.1. X-ray diffraction

X-ray diffraction patterns of LiV_3O_8 and $LiNi_{1/3}Co_{1/3}Mn_{1/3}O_2$ are plotted in Fig. 1. LiV_3O_8 has good crystalline structure and is assigned to monoclinic phase with space group of *P*21/*m* (JCPDS 72–1193). The structure is composed of VO_6 octahedron and VO_5 distorted trigonal bi-pyramids. The assignment of major peaks are in good agreement with previous studies [22–24]. A small impurity peak belonging to $Li_{0.2}V_2O_5$ is noticed at 12.3°. As for $LiNi_{1/3}Co_{1/3}Mn_{1/3}O_2$, the pattern fits perfectly with hexagonal α-$NaFeO_2$ phase with space group of *R*-3 m [25,26]. The well-splittings of (006)/(102) and (018)/(110) peaks reveal good crystalline ordering in the hexagonal structure. Additionally, the intensity ratio of (003) peak to (104) peak is 1.47, indicating that Li^+/Ni^{+2} cation intermixing is very low.

3.2. X-ray photoelectron spectroscopy

The oxidation states of Mn, Ni and Co elements in $LiNi_{1/3}Co_{1/3}Mn_{1/3}O_2$ and V element in LiV_3O_8 were determined by X-ray photoelectron spectroscopy measurements and the results are shown in Fig. 2. The Co 2p spectrum has two main peaks, $2p_{3/2}$ peak at 780.0 eV and $2p_{1/2}$ peak at 795.0 eV with a separation of 15 eV. These binding energies correspond to Co^{3+} [26,27]. The XPS curve fitting revealed the coexistence of Co^{4+} which is validated by the peaks

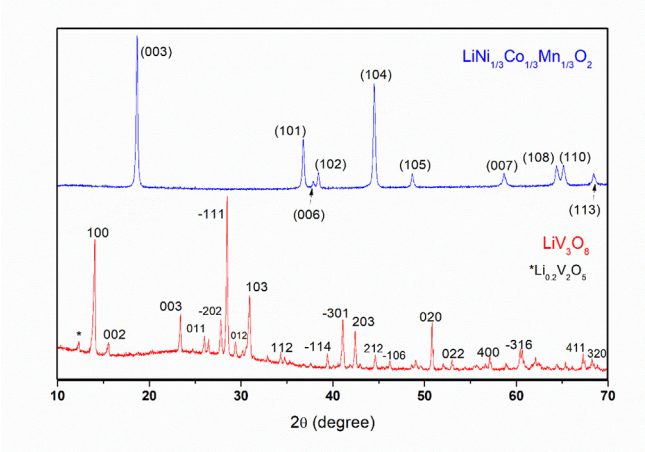

Fig. 1. X-ray diffraction patterns of $LiNi_{1/3}Co_{1/3}Mn_{1/3}O_2$ and LiV_3O_8 materials

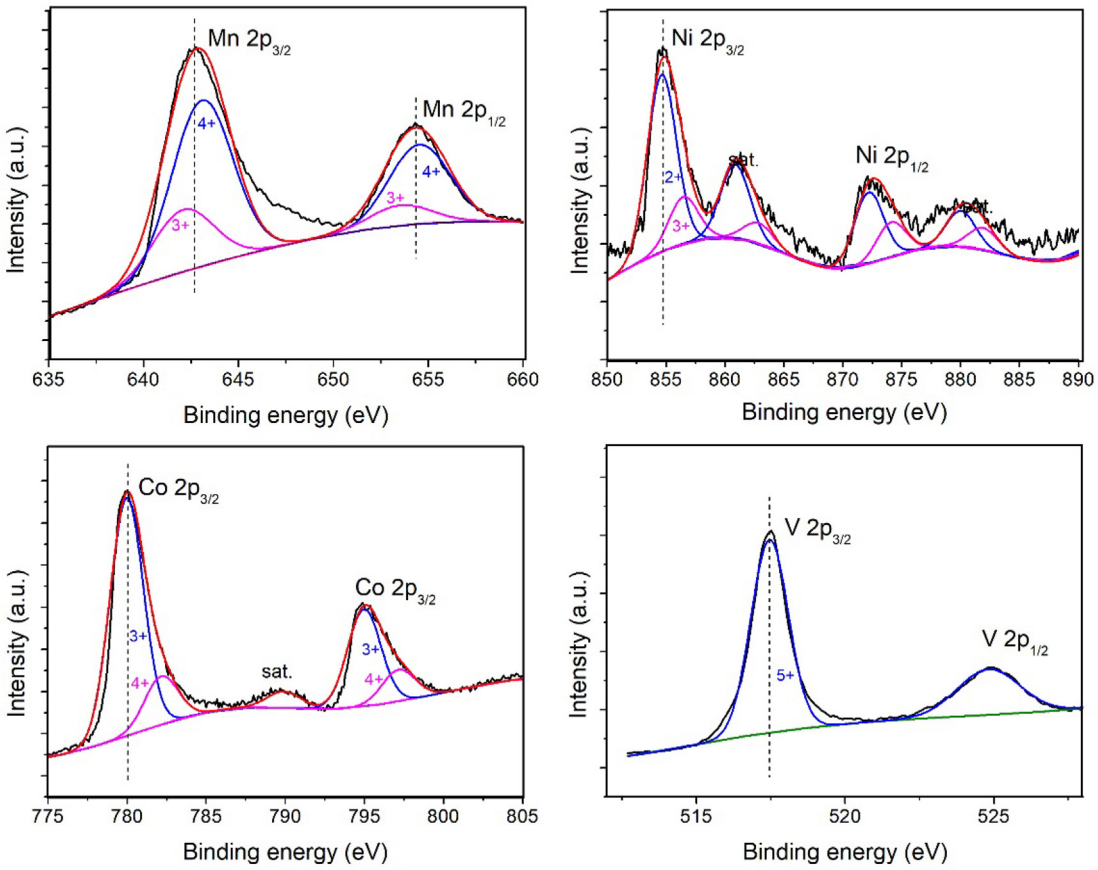

Fig. 2. XPS spectra of Mn, Ni and Co elements in $LiNi_{1/3}Co_{1/3}Mn_{1/3}O_2$ and V element in LiV_3O_8.

located at 782.2 and 797.2 eV. The Mn spectrum has two main peaks, $2p_{3/2}$ peak at 642.8 eV and $2p_{1/2}$ peak at 654.3 eV, representing Mn^{4+} cation [28]. Besides Mn^{4+}, a smaller quantity of Mn^{3+} also exists with its peaks located at 641.8 and 653.3 eV. In Ni spectrum, two dominant peaks located at 854.7 and 872.3 eV are observed, which match $2p_{3/2}$ and $2p_{3/2}$ orbitals of Ni^{2+} [29]. Besides these, two satellite peaks located at 861.0 and 879.5 eV are also noticed and they further confirm Ni^{2+} oxidation state. However, the best XPS fitting was realized by placing four weaker peaks. These peaks are positioned about 2.0 eV to the right of Ni^{2+} peaks and represent Ni^{3+} oxidation state. The presence of mixed oxidation states resulting from electron transfer between different cations was reported previously for $LiNi_{1/3}Co_{1/3}Mn_{1/3}O_2$ material [29]. As for V spectrum, two main peaks at 517.5 and 524.85 eV are observed, which correspond to V^{5+}.

3.3. Scanning electron microscopy

Fig. 3. illustrates scanning electron microscope images of LiV_3O_8 and $LiNi_{1/3}Co_{1/3}Mn_{1/3}O_2$. LiV_3O_8 sample is made of stick-like particles with an aspect ratio of 3–5. The longer side is a few micrometers in length, while the shorter side is 0.5–1 μm. This stick-like morphology was reported previously for LiV_3O_8 [30]. The particles appear to have a smooth surface. This suggests good crystallinity of the material and it is conducive to lithium movement in and out of anode material. On the other hand, $LiNi_{1/3}Co_{1/3}Mn_{1/3}O_2$ is composed of interconnected nanoparticles having a diameter of 200–300 nm. The particle size seems to be uniformly distributed and there is no sign of aggregation. While such a small size is favorable to lithium kinetics, it poses a greater risk for electrolyte oxidation due to greater overall surface area.

3.4. Electrochemical testing

Charge-discharge voltage profiles of LiV_3O_8 electrode in aqueous water-in-salt electrolyte (i.e. 20 M LiTFSI in H_2O) are displayed in Fig. 4a. In order to gain a general sense of the cyclability of anode material in aqueous electrolyte, the discharge cut-off voltage was limited to −0.25 V vs. Ag/AgCl. Also, the cycle number was restricted to 5 cycles in order not to degrade electrolyte too much due to the use of non-sacrificial Pt counter electrode. The profile consists of a sloping line down to −0.15 V (marked by the arrow) followed by a plateau around −0.2 V. These regions were described as single-phase and two-phase transformations, respectively based on X-ray diffraction analysis [31]. The first region reaches a capacity of about 90 mAh g^{-1}, thereby corresponding to intercalation of 1Li atom into LiV_3O_8 (LiV_3O_8 has a theoretical capacity of 282 mAh g^{-1} assuming 3Li per LiV_3O_8). Here, V^{5+} is reduced to V^{4+} [31]. In the plateau region, the lithium capacity increases to 135.4 mAh g^{-1}, indicating that another 0.5Li atom is intercalated into the host structure. In the first charge cycle, the delithiation capacity is as high as 147.6 mAh g^{-1}. The reason behind more than 100% coulombic efficiency is that some of the pre-existing lithium ions in as-synthesized material leave the electrode material during the first delithiation step. The difference in average charge and discharge potentials is relatively small at 57 mV. However, LiV_3O_8 suffers a 9% capacity loss in the next cycles. While this suggests a fast capacity decay, it can be noticed upon a more detailed look at the voltage profiles that the capacity loss mostly comes from the plateau region. This behavior was reported previously and large changes in lattice parameters *a* and *b* associated with the two-phase region were described as potential culprits behind the decrease in cyclability [32].

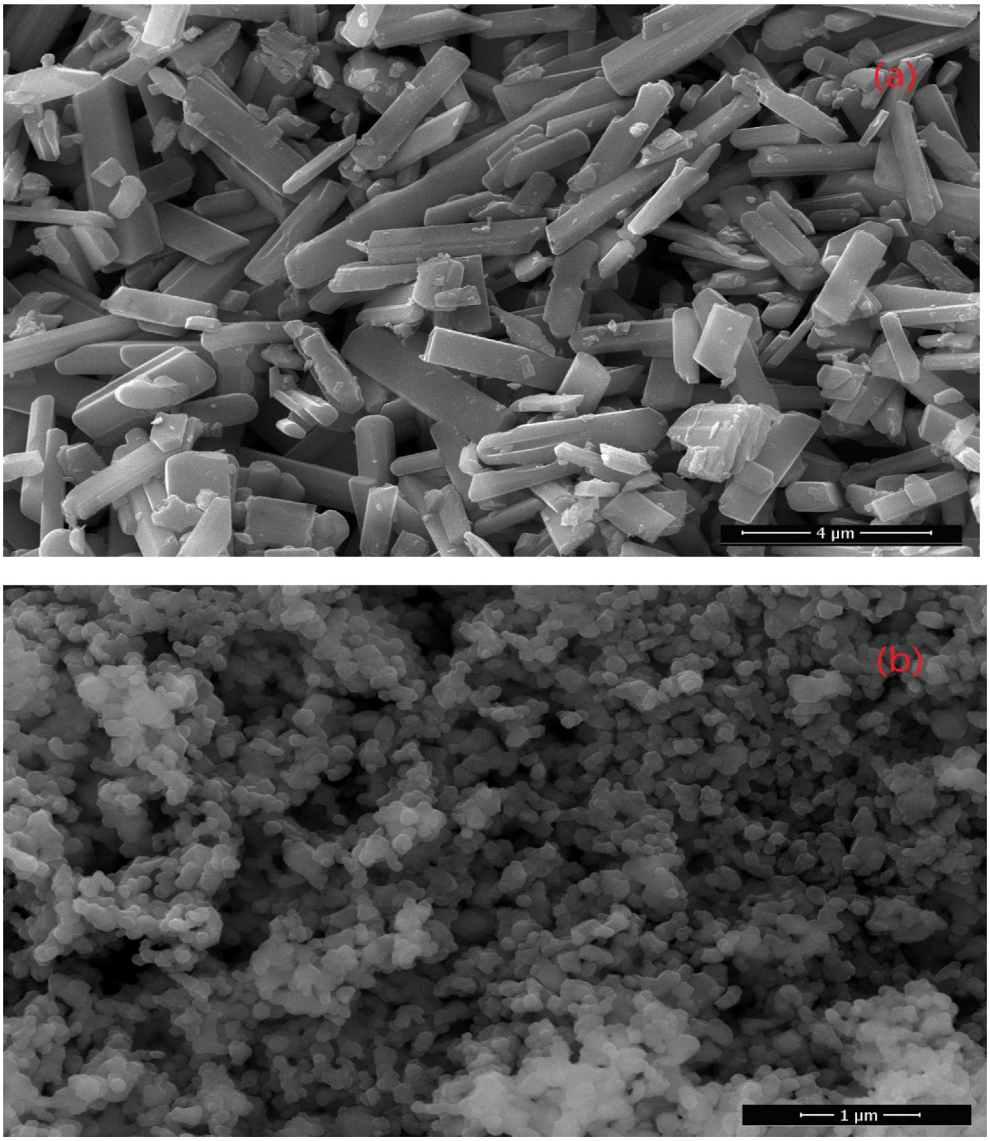

Fig. 3. SEM images of (a) LiV_3O_8 and (b) $LiNi_{1/3}Co_{1/3}Mn_{1/3}O_2$ powders.

Cyclic voltammetry scans of LiV_3O_8 electrode were collected between the same potential range to gather more information about its cyclability in 'water-in-salt' aqueous electrolyte. The profiles are plotted in Fig. 4b. The arrow on the cathodic side of the figure points to the transition from single-phase to two-phase reaction. After this point, a cathodic peak around −0.20 V vs. Ag/AgCl is noticed. This peak is located at −0.05 V vs. Ag/AgCl on the anodic scan. It is unambiguously clear that this peak belonging to the two-phase transformation is largely irreversible. On the other hand, the single-phase region consists of many small peaks with high reversibility, in particular starting with the third cycle. The good agreement between the galvanostatic and cyclic voltammetry profiles indicates that the lithiation capacity of LiV_3O_8 anode should be limited to 1Li atom to achieve good cyclability. In order to determine whether such a limitation exists due to some kind of interaction between LiV_3O_8 electrode and 'water-in-salt' aqueous electrolyte, LiV_3O_8 was also tested in half cells against Li metal using non-aqueous organic carbonate electrolyte. The voltage profiles for the first 20 cycles are given in Fig S1. It is observed that the two-phase plateau also exhibits poor reversibility in the non-aqueous electrolyte. However, significant improvement in cyclability is achieved when the discharge cut-off voltage is limited to 2.6 V vs. Li/Li^+ (i.e. 1Li atom per LiV_3O_8). Therefore, this result proves that LiV_3O_8 is stable in 20 M LiTFSI electrolyte and can be cycled with good reversibility if lithiation capacity does not exceed 1Li atom per LiV_3O_8.

Prior to making full cells, $LiNi_{1/3}Co_{1/3}Mn_{1/3}O_2$ cathode was also tested against Pt electrode in 20 M LiTFSI electrolyte (Fig. 4c). The voltage profile of cathode includes a low voltage pseudo-plateau and a high voltage steep curve consistent with earlier studies conducted in organic electrolytes (i.e. 1 M $LiPF_6$ in EC-DEC) [33]. The charge and discharge capacities in the first cycle are 169 and 147 mAh g^{-1}, respectively. The coulombic efficiency corresponds to 87%, which is a high number even for organic electrolytes. A sister electrode tested to confirm this result yielded an even better first cycle coulombic efficiency as high as 90% (Fig. S2). The loss in capacity in the fifth cycle was only around 2%. Finally, the difference in average charge and discharge potentials is only 49 mV, which suggests low polarization in the cell. It is widely known that the surface of nickel-based cathode materials transforms into rock-salt type phase upon exposure to humidity. Our battery results prove that $LiNi_{1/3}Co_{1/3}Mn_{1/3}O_2$ exhibits good structural stability in 'water-in-salt' electrolyte and its battery performance far exceeds previous reports performed in other aqueous electrolytes.

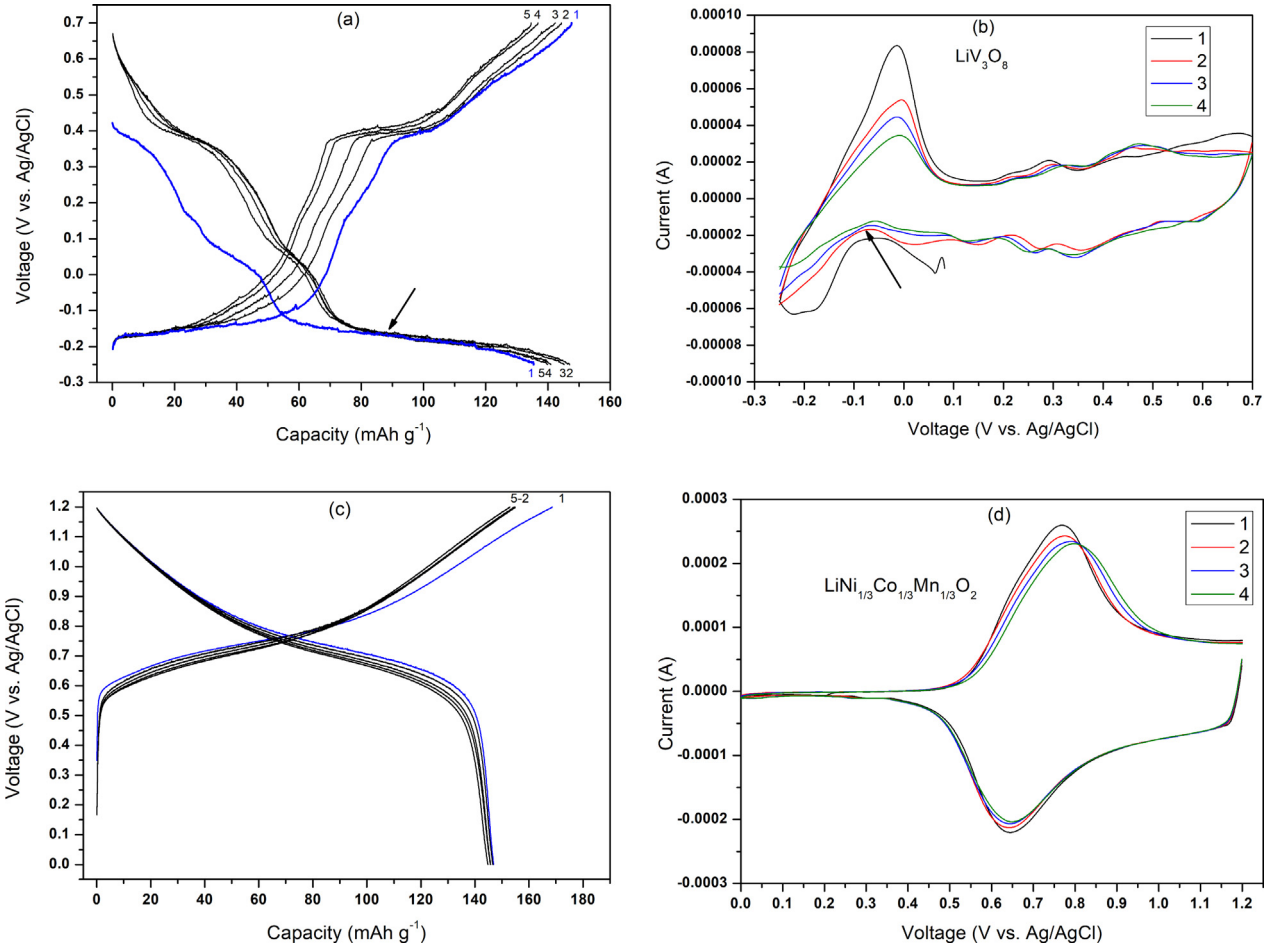

Fig. 4. (a) Voltage vs. capacity curves of LiV_3O_8 vs. Pt in aqueous 20 M LiTFSI-H_2O (b) its cyclic voltammetry scans in the first four cycles (c) Voltage vs. capacity curves of $LiNi_{1/3}Co_{1/3}Mn_{1/3}O_2$ vs. Pt in aqueous 20 M LiTFSI-H_2O (d) its cyclic voltammetry scans in the first four cycles. The arrows mark the limiting potentials for the lithiation of LiV_3O_8 anode.

The lithiation/delithiation mechanism of $LiNi_{1/3}Co_{1/3}Mn_{1/3}O_2$ cathode was also investigated using cyclic voltammetry. The anodic and cathodic scans are displayed in Fig. 4d. A single cathodic peak at −0.65 V vs. Ag/AgCl and a matching anodic peak at 0.77 V vs. Ag/AgCl are seen in the first cycle. These peaks are identical to those seen in non-aqueous electrolytes [34] which proves that the mechanism of lithium intercalation and extraction did not change with the use of aqueous solution. The peaks become slightly smaller in intensity in the next 3 cycles due to some capacity loss as typically seen in electrode materials. Overall, it can be stated that $LiNi_{1/3}Co_{1/3}Mn_{1/3}O_2$ shows very good reversibility in 20 M LiTFSI electrolyte.

Assuming a delithiation capacity of 169 mAh g^{-1} for the $LiNi_{1/3}Co_{1/3}Mn_{1/3}O_2$ cathode and a maximum lithiation capacity of 90 mAh g^{-1} for the LiV_3O_8 anode (in order to extend the cyclability of LiV_3O_8 as argued above), a minimum anode-to-cathode weight ratio of 1.88 is calculated. If the ratio used in the full cell is significantly above this value, the cyclability of full cell would be enhanced due to lesser amount of lithium ions intercalating into anode material. But, this would come at the expense of full cell energy density due to inefficient use of anode. If a ratio below this value is used in full cell, more than 1Li atom per LiV_3O_8 would be forced into the anode material and its cyclability would be jeopardized. With all these in consideration, anode-to-cathode mass ratio of 2.26 was used in our cell, a reasonable 20% more than the minimum value. The electrochemical results belonging to LiV_3O_8 / 20 M LiTFSI in H_2O / $LiNi_{1/3}Co_{1/3}Mn_{1/3}O_2$ full cell are given in Fig. 5.

The voltage vs. capacity curves of the full cell are shown in Fig. 5a for 1st, 2nd, 10th and 100th cycles. Other than the low voltage segment, the profile resembles that of the cathode electrode. The first cycle coulombic efficiency is 80% and it is 7% less than it was with $LiNi_{1/3}Co_{1/3}Mn_{1/3}O_2$. There might be two potential reasons behind lower efficiency in full cell. The first reason is that cathode material might have been charged to above 1.2 V vs. Ag/AgCl in full cell, which was the cut-off voltage in half cell measurements. The larger charging voltage could result in more electrolyte oxidation, thereby causing irreversibility. Since it is challenging to control anode and cathode potential individually in a full cell, more optimization is required to obtain the best performance. The second reason is that 0.2 V discharge cut-off voltage may not be enough to fully lithiate the cathode material. The coulombic efficiency of full cell can be seen to reach 96% in the second cycle and stabilizes around 99–100% at extended cycling (Fig. 5b). Such high numbers indicate that active materials form a stable solid-electrolyte interface quickly and side reactions diminish with time.

The variaton of the specific charge and discharge capacities of LiV_3O_8 and $LiNi_{1/3}Co_{1/3}Mn_{1/3}O_2$ materials as a function of cycle number are provided in Fig. 5c. These capacities were calculated by dividing the full cell charge and discharge capacities of the full cell (Fig. 5b) to the mass of corresponding active material (6.16 mg for LiV_3O_8 and 2.12 mg for $LiNi_{1/3}Co_{1/3}Mn_{1/3}O_2$). The first cycle charge (delithiation) and discharge (lithiation) capacities of $LiNi_{1/3}Co_{1/3}Mn_{1/3}O_2$ cathode are 182.2 mAh g^{-1} and 145.8 mAh g^{-1}. As mentioned above,

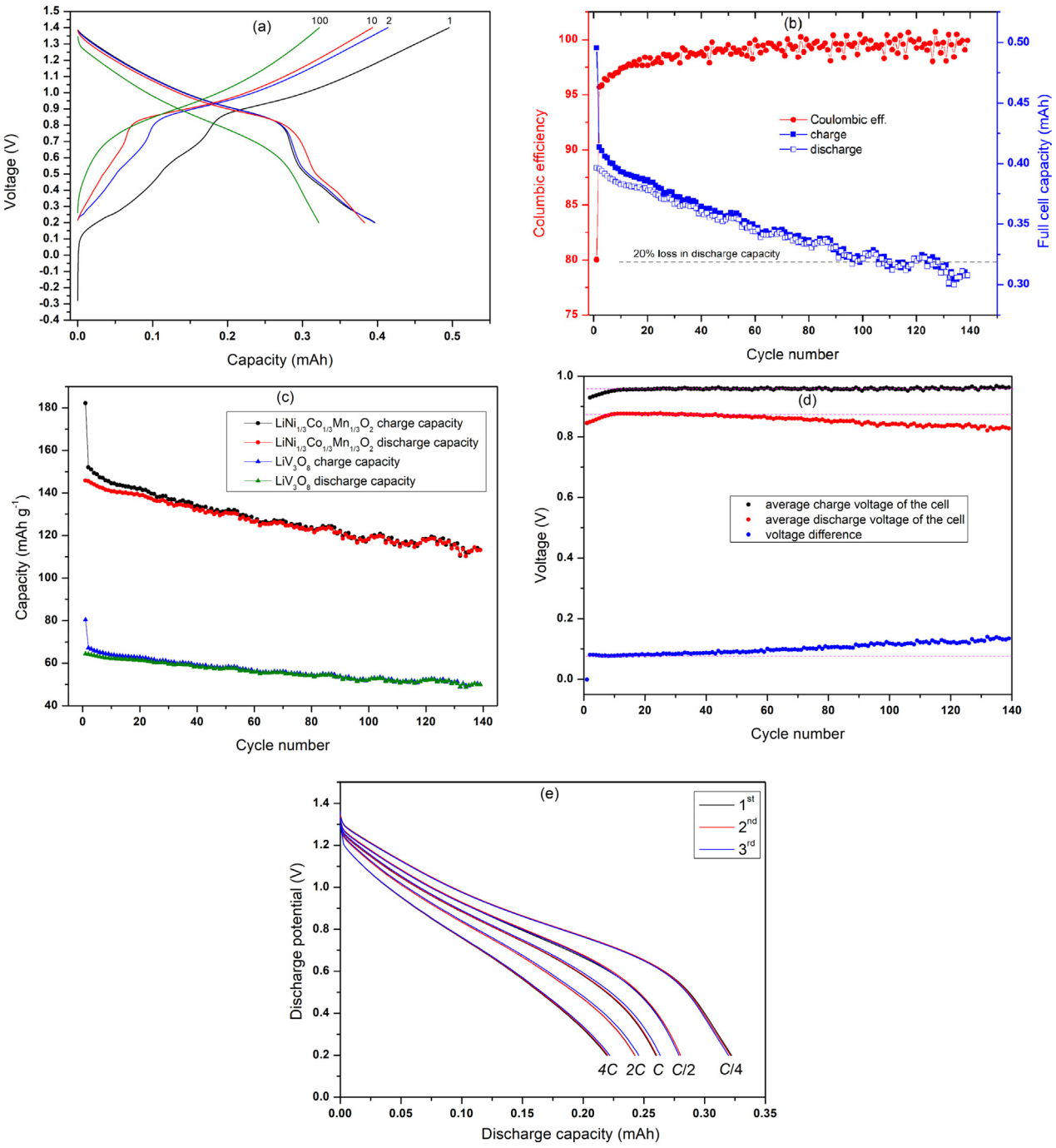

Fig. 5. Battery data of a 2032 coin cell containing LiV_3O_8 as anode, $LiNi_{1/3}Co_{1/3}Mn_{1/3}O_2$ as cathode and 'water-in-salt' 20 M LiTFSI as electrolyte. (a) Voltage vs. capacity profiles of the full cell in the first 100 cycles (b) Coulombic efficiency of the full cell and its charge and discharge capacities (c) Gravimetric capacities of anode and cathode active materials in the full cell (d) Average charge and discharge potentials of the full cell (e) The discharge voltage profiles of the full cell at varying discharge rates. The 1st, 2nd and 3rd refer to cycle numbers.

all of the charge capacity may not come from the delithiation of cathode material but also partially from the oxidation of aqueous electrolyte. The discharge capacity is very close to that obtained in half cell measurements. Similarly, the charge (lithiation) capacity of LiV_3O_8 is 80 mAh g^{-1}, which stayed below our 90 mAh g^{-1} threshold thanks to the use of larger anode-to-cathode mass ratio. On the delithiation step, only 64.5 mAh g^{-1} capacity leaves the anode. The half cell measurements showed that LiV_3O_8 can have first cycle coulombic efficiency over unity. The reason for leftover lithium in LiV_3O_8 can be explained by the poor reversibility of cathode material in the first cycle. The critical threshold value for 20% capacity loss is seen to take place between 100th-110th cycles. To our best knowledge, this is the longest cycle life reported in any LiV_3O_8/layered cathode couple in literature.

The average charge and discharge potentials of the full cell were calculated by dividing the energy of the cell (mWh) to the capacity of the cell (mAh). The results are shown in Fig. 5d. The average potentials for charge and discharge steps startat 0.929 V and 0.849 V in the second cycle, respectively. The 80 mV polarization in the full cell is slightly less than the summation of half cell polarizations, namely

57 mV for LiV_3O_8 and 49 mV for $LiNi_{1/3}Co_{1/3}Mn_{1/3}O_2$. The polarization difference might be attributed to the contribution from Li de/plating during half cell measurements. After stabilizing at 0.957 V and 0.876 V in the next 40 cycles, the discharge potential slips to 0.83 V at the end of 140th cycle while the charge potential remains same at 0.96 V. The stability of cell potentials during extended cycling indicates that there is no significant polarization build-up in the full cell. Based on cell discharge potential, cell capacity and total active material mass, the energy density of the cell in the first cycle is calculated to be 38 Whkg^{-1} (0.849 V * 0.396 mAh / 8.88 mg). It is our opinion that this number can be easily increased to 60 Wh kg^{-1} with further improvement in anode capacity as it appears to be the bottleneck. The resulting cell could rival other aqueous chemistries including lead-acid batteries.

The rate performance of the full cell was evaluated at *C*/4, *C*/2, 1*C*, 2*C* and 4*C* discharge rates and the discharge voltage profiles are plotted in Fig. 5e. At least three measurements were taken for each rate. It is seen that the full cell delivers acceptable capacities even at higher rates. Specifically, the capacities at *C*/2, 1*C*, 2*C* and 4*C* are respectively 87%, 81%, 75% and 68% of the one at *C*/4. Since discharge rate performance of the full cell is dependent on both the lithiation kinetics of $LiNi_{1/3}Co_{1/3}Mn_{1/3}O_2$ cathode and delithiation kinetics of LiV_3O_8 anode, further improvements in rate capability rely on developing each active material simultaneously. On the other hand, the aqueous electrolyte used in this study is known to have higher viscosity and lower lithium conductivity than standard organic carbonate solvents [35]. This might constitute a major hurdle in increasing the power density of the full cell.

Partial replacement of V^{5+} ions by other metals can be explored to extend the lithium capacity of LiV_3O_8 anode beyond 1Li atom. A range of elements including Nb^{5+} [36], Mo^{6+} [37], B^{3+} [38], Si^{4+} [39] have been doped into LiV_3O_8 and significant improvements in gravimetric capacity and cyclability were reported. It was speculated that as larger dopant ion substituted smaller V^{5+} ion, the lattice volume of LiV_3O_8 was enlarged and the stability of the crystal structure was increased. This mechanism resulted in improved reversibility of phase transformations betwen initial LiV_3O_8 and fully lithiated $Li_4V_3O_8$ phases. Morales et al., [40] declared LiV_3O_8 unsuitable as an electrode for aqueous batteries based on the dissolution of vanadium into the electrolyte in the form of VO_2^+ ions. The electrochemical testing was performed in 1 M $LiNO_3$ electrolyte and the initially colorless electrolyte turned yellowish and LiV_3O_8 suffered a very rapid capacity decay. In order to repeat their results, we also tested our anode in 5 M $LiNO_3$ aqueous solution. The electrolyte turned yellow (Fig. S3a) and LiV_3O_8 lost 80% of its capacity after only 9 cycles (Fig. S3b). On the other hand, no color change was observed in novel 'water-in-salt' 20 M LiTFSI electrolyte and capacity retention was remarkably better. Holze et al., [14] reported that the reversibility of LiV_3O_8 was enhanced upon coating with a thin layer of polypyrrole polymer. It was stated that the coating protected the electrode material against harmful effects of H_2O molecules, resulting in lesser amount of vanadium dissolution into the electrolyte. Since there are much reduced number of free water molecules in 'water-in-salt' electrolyte, their results agree perfectly with ours and explain the enhancement in the cyclability of LiV_3O_8 electrode over those in lower molarity nitrate or sulphate-based aqueous electrolytes. The coating of LiV_3O8 with a thin layer of a conducting polymer might be another remedy to improve the stability and performance of this anode material [41].

As for $LiNi_{1/3}Co_{1/3}Mn_{1/3}O_2$ cathode, the major causes of capacity loss can be attributed to the growth of solid-electrolyte interface and irreversible phase transformations near the surface of cathode particle. Its cyclability in an aqueous electrolyte can be significantly prolonged by utilizing a few simple strategies. They include the use of primary particles several micrometer in diameter as opposed to nano-sized ones used in this study, the coating of cathode surface with a thin layer of inert oxide and the use of a concentration gradient cathode with the Ni-poor region near particle surface. All these measures can help mitigate the harmful effects of aqueous electrolyte and also stabilize the active material surface. In our future work, we intend to pursue these avenues to realize further gains in energy density and cyclability of our full cell.

4. Conclusion

The demonstration of LiV_3O_8/$LiNi_{1/3}Co_{1/3}Mn_{1/3}O_2$ couple in 'water-in-salt' 20 M LiTFSI electrolyte was reported for the first time in literature. In the first cycle, specific delithiation capacity of LiV_3O_8 anode was 64.5 mAh g^{-1} while the specific lithiation capacity of $LiNi_{1/3}Co_{1/3}Mn_{1/3}O_2$ was 145.8 mAh g^{-1}. These numbers are significantly higher than those in previous studies performed using aqueous $LiNO_3$ and Li_2SO_4 electrolytes. Since the salt concentration in 'water-in-salt' electrolyte is significantly larger than those in typical electrolytes, this results in much reduced number of free water molecules in the former. This fact reduces the amount of side reactions between active materials and water solvent. Specifically, vanadium dissolution into the aqueous electrolyte is eliminated. Also, the detrimental phase transformation (layered to rock salt) taking place on the surface of cathode material upon exposure to water is circumvented, as demonstrated in the preceding paper. In our future work, we will focus on increasing the lithium capacity of LiV_3O_8 anode and the cyclability of $LiNi_{1/3}Co_{1/3}Mn_{1/3}O_2$ cathode.

CRediT authorship contribution statement

Muharrem Kunduraci: Conceptualization, Funding acquisition, Investigation, Writing – original draft. **Selda Kilic Cetin:** Investigation. **Ugur Caglayan:** Investigation. **Rasiha Nefise Mutlu:** Data curation. **Dogan Kaya:** Investigation. **Ahmet Ekicibil:** Resources, Writing – review & editing.

Declaration of competing interest

The authors declare that they have no known competing financial interests or personal relationships that could have appeared to influence the work reported in this paper.

Acknowledgements

This work received financial support from TÜBİTAK under the project number of 217M113.

Appendix A. Supplementary data

Supplementary data to this article can be found online at https://doi.org/10.1016/j.jelechem.2022.116118.

References

[1] W. Meng, C. Li, M. Yao, Z. He, X. Wu, Z. Jiang, L. Dai, L. Wang, Synthesis and electrochemical performance of $Li_{1+x}Ti_{2-x}Fe_x(PO_4)_3$/C anode for aqueous lithium ion battery, Adv. Powder Tech. 31 (2020) 1359–1364.
[2] L. Sharma, K. Nakamoto, S. Okada, P. Barpanda, Tavorite $LiFePO_4OH$ hydroxyphosphate as an anode for aqueous lithium-ion batteries, J. Power Sources 429 (2019) 17–21.
[3] Y. Wang, S.-Z. Yang, Y.a. You, Z. Feng, W. Zhu, V. Gariépy, J. Xia, B. Commarieu, A. Darwiche, A. Guerfi, K. Zaghib, High-capacity and long-cycle life aqueous rechargeable lithium-ion batterywith the $FePO_4$ anode, ACS Appl. Mater. Interfaces 10 (8) (2018) 7061–7068.
[4] L. Suo, F. Han, X. Fan, H. Liu, K. Xu, C. Wang, Water-in-salt electrolytes enable green and safe Li-ion batteries for large scale electric energy storage applications, J. Mater. Chem. A 4 (17) (2016) 6639–6644.
[5] D. Zhou, S. Liu, H. Wang, G. Yan, $Na_2V_6O_{16}$-0.14H_2O nanowires as novel anode material for aqueois rechargeable lithium battery with good cycling performance, J. Power Sources 227 (2013) 111–117.

[6] L.i. Liu, M. Zhou, X. Wang, F. Tian, H. Guo, B. Shen, T. Hu, Improvement of electrochemical properties of $LiV_3O_8/LiMn_2O_4$ ARLB by NiO nanofibers coating on the anode, J. Electrochem. Soc. 159 (8) (2012) A1230–A1235.
[7] M. Zhao, Q. Zheng, F. Wang, W. Dai, X. Song, Electrochemical performance of high specific capacity of lithium-ion cell $LiV_3O_8/LiMn_2O_4$with $LiNO_3$ aqueous solution electrolyte, Electrochim. Acta 56 (2011) 3781–3784.
[8] C.H. Mi, X.G. Zhang, H.L. Li, Electrochemical behaviors of solid $LiFePO_4$ and $Li_{0.99}Nb_{0.01}FePO_4$ in Li_2SO_4 aqueous electrolyte, J. Electroanal. Chem. 602 (2) (2007) 245–254.
[9] X. Zhong, F. Wang, Y. Ding, L. Duan, F. Shi, C. Wang, Water-in-salt electrolyte Zn/$LiFePO_4$ batteries, J. Electroanal. Chem. 867 (2020) 114193.
[10] W.u. Li, J.R. Dahn, D.S. Wainwright, Rechargeable lithium batteries with aqueous electrolytes, Science 264 (5162) (1994) 1115–1118.
[11] M. Kunduraci, R.N. Mutlu, A.M. Gizir, Electrochemical behavior of $LiNi_{0.6}Co_{0.2}Mn_{0.2}O_2$ cathode in different aqueous electrolytes, Ionics 26 (2020) 1663–1672.
[12] L. Zhu, L. Xie, X. Cao, LiV_3O_8/Polydiphenylamine composites with significantly improved electrochemical behavior as cathode materials for rechargeable lithium batteries, ACS Appl. Mater. Interface 10 (2018) 10909.
[13] W. Wu, J. Ding, H. Peng, G. Li, Synthesis and electrochemical properties of single-crystalline LiV_3O_8 nanobelts for rechargeable lithium batteries, Mater. Lett. 65 (14) (2011) 2155–2157.
[14] L.L. Liu, X.J. Wang, Y.S. Zhu, C.L. Hu, Y.P. Wu, R. Holze, Polypyrole-coated LiV_3O_8-nanocomposites with good electrochemical performance as anode material for aqueous rechargeable lithium batteries, J. Power Sources 224 (2013) 290–294.
[15] J. Liu, L. Yi, L.i. Liu, P. Peng, LiV_3O_8 nanowires with excellent stability for aqueous rechargeable lithium batteries, Mater. Chem. Phys. 161 (2015) 211–218.
[16] G.J. Wang, N.H. Zhao, L.C. Yang, Y.P. Wu, H.Q. Wu, R. Holze, Characteristics of an aqueous rechargeable lithium battery, ARLB, Electrochim. Acta 52 (2007) 4911–4915.
[17] H. Yadegari, A. Jabbari, H. Heli, An aqueous rechargeable lithium-ion battery based on $LiCoO_2$ nanoparticles cathode and LiV_3O_8 nanosheets anode, J. Solid State Electrochem. 16 (1) (2012) 227–234.
[18] G.J. Wang, L.J. Fu, B. Wang, N.H. Zhao, Y.P. Wu, R. Holze, An aqueous rechargeable lithium battery based on $LiV_3O_8$and $Li[Ni_{1/3}Co_{1/3}Mn_{1/3}]O_2$, J. Appl. Electrochem. 38 (4) (2008) 579–581.
[19] L. Liu, F. Tian, Z. Yang, X. Wang, M. Zhou, X. Wang, Electrochemical behavior nanostructured LiV_3O_8 in aqueous $LiNO_3$ solution, J. Phys. Chem. Solids 72 (2011) 1495–1500.
[20] J. Köhler, H. Makihara, H. Uegaito, H. Inoue, M. Toki, LiV_3O_8: characterization as anode material for an aqueous rechargeable Li-ion battery system, Electrochim. Acta 46 (2000) 59–65.
[21] L. Suo, O. Borodin, T. Gao, M. Olguin, J. Ho, X. Fan, C. Luo, C. Wang, K. Xu, 'Water-in-salt' electrolyte enables high-voltage aqueous lithium-ion chemistries, Science 350 (6263) (2015) 938–943.
[22] X. Xiong, Z. Wang, X. Li, H. Guo, Study on ultrafast synthesis of LiV_3O_8 cathode material for lithium-ion batteries, Mater. Lett. 76 (2012) 8–10.
[23] A. Pan, J. Liu, J.-G. Zhang, G. Cao, W.u. Xu, Z. Nie, X. Jie, D. Choi, B.W. Arey, C. Wang, S. Liang, Template free synthesis of LiV_3O_8 nanorods as a cathode material for high-rate secondary lithium batteries, J. Mater. Chem. 21 (4) (2011) 1153–1161.
[24] W. Li, L. Zhu, Z. Yu, L. Xie, X. Cao, LiV_3O_8/polytriphenylamine composites with enhanced electrochemical performances as cathode materials for rechargeable lithium batteries, Materials 10 (2017) 344–356.
[25] X.-Y. Qiu, Q.-C. Zhuang, Q.-Q. Zhang, R.u. Cao, Y.-H. Qiang, P.-Z. Ying, S.-G. Sun, Investigation of layered $LiNi_{1/3}Co_{1/3}Mn_{1/3}O_2$ cathode of lithium ion battery by electrochemical impedance spectroscopy, J. Electroanal. Chem. 687 (2012) 35–44.
[26] F. Xu, H. Yan, J. Chen, Z. Zhang, C. Fan, Improving electrochemical properties of $LiNi_{1/3}Co_{1/3}Mn_{1/3}O_2$ by enhancing thermal decomposition of carbonates to synthesize ultrafine powders, J. Electroanal. Chem. 820 (2018) 118–122.
[27] S.J. Shi, J.P. Tu, Y.Y. Tang, Y.Q. Zhang, X.Y. Liu, X.L. Wang, C.D. Gu, Enhanced electrochemical performance of LiF-modified $LiNi_{1/3}Co_{1/3}Mn_{1/3}O_2$cathode materials for Li-ion batteries, J. Power Sources 225 (2013) 338–346.
[28] Z. Lu, Y. Liu, X. Lu, H. Wang, G. Yang, Y. Chao, W. Li, F. Yin, An active core-shell nanoscale design for high voltage cathode of lithium storage devices, J. Power Sources 360 (2007) 409–418.
[29] K.M. Shaju, G.V. Subba Rao, B.V.R. Chowdari, Performance of layered $LiNi_{1/3}Co_{1/3}Mn_{1/3}O_2$as cathode for Li-ion batteries, Electrochim. Acta 48 (2) (2002) 145–151.
[30] K.Y. Bae, Y.H. Jung, S.H. Cho, B.H. Kim, W.Y. Yoon, Design and analysis of an optimal cathode for Li-LiV_3O_8 secondary cells, J. Alloys Compd. 784 (2019) 704–711.
[31] S. Maletti, A. Sarapulova, A.A. Tsirlin, S. Oswald, F. Fauth, L. Giebeler, N.N. Bramnik, H. Ehrenberg, D. Mikhailova, Electrochemical behavior of LiV_3O_8 positive electrode in hybrid Li, Na-ion batteries, J. Power Sources 373 (2018) 1–10.
[32] S. Jouanneau, A. Salle, A. Verbaere, D. Guyomard, The origin of capacity fading upon lithium cycling in $Li_{1.1}V_3O_8$, J. Electrochem. Soc. 152 (2005) A1660–A1667.
[33] L. Zhu, C. Bao, L. Xie, X. Yang, X. Cao, Review of synthesis and structural optimization of $LiNi_{1/3}Co_{1/3}Mn_{1/3}O_2$ cathode materials for lithium-ion battery applications, J. Alloys Compd. 831 (2020) 154864.
[34] Q. Jing, J. Zhang, C. Yang, Y. Chen, C. Wang, A novel and practical hydrothermal method for synthesizing $LiNi_{1/3}Co_{1/3}Mn_{1/3}O_2$ cathode material, Cer. Int. 46 (12) (2020) 20020–20026.
[35] O. Borodin, L. Suo, M. Gobet, X. Ren, F. Wang, A. Faraone, J. Peng, M. Olguin, M. Schroeder, M.S. Ding, E. Gobrogge, A. von Wald Cresce, S. Munoz, J.A. Dura, S. Greenbaum, C. Wang, K. Xu, Liquid structure with nano-heterogeneity promotes cationic transport in concentrated electrolytes, ACS Nano 11 (10) (2017) 10462–10471.
[36] L. Wang, L. Deng, Y. Li, X. Ren, H. Mi, L. Sun, P. Zhang, Y. Gao, Nb^{5+} doped LiV_3O_8 nanorods with extraordinary rate performance and cycling stability as cathodes for lithium-ion batteries, Electrochim. Acta 284 (2018) 366–375.
[37] H. Song, Y. Liu, C. Zhang, C. Liu, G. Cao, Mo-doped LiV_3O_8 nanorod-assembled nanosheets as a high performance cathode material for lithium ion batteries, J. Mater. Chem. A 3 (7) (2015) 3547–3558.
[38] Y. Feng, Y. Li, F. Hou, Boron doped lithium trivanadate as a cathode material for an enhanced rechargeable lithium batteries, J. Power Sources 187 (2009) 224–228.
[39] M. Zhao, L. Jiao, H. Yuan, Y. Feng, M. Zhang, Study on the silicon doped lithium trivanadate as cathode material for rechargeable lithium batteries, Solid State Ionics 178 (5-6) (2007) 387–391.
[40] A. Caballero, J. Morales, O.A. Vargas, Electrochemical instability of LiV_3O_8 as an electrode material for aqueous rechargeable lithium batteries, J. Power Sources 195 (13) (2010) 4318–4321.
[41] V.L. Martins, T.T. Obana, R.M. Torresi, Electroactivity of 3D conducting polymers in water-in-salt electrolyte and their electrochemical capacitor performance, J. Electroanal. Chem. 880 (2021) 114822.